Emerging Topics in Life Sciences (2021) **5** 61–75
https://doi.org/10.1042/ETLS20200354

PORTLAND PRESS

Review Article

Spectroscopy of model-membrane liposome-protein systems: complementarity of linear dichroism, circular dichroism, fluorescence and SERS

Anastasiia Tukova and Alison Rodger

Macquarie University, Sydney, Australia

Correspondence: Alison Rodger (alison.rodger@mq.edu.au)

A range of membrane models have been developed to study components of cellular systems. Lipid vesicles or liposomes are one such artificial membrane model which mimics many properties of the biological system: they are lipid bilayers composed of one or more lipids to which other molecules can associate. Liposomes are thus ideal to study the roles of cellular lipids and their interactions with other membrane components to understand a wide range of cellular processes including membrane disruption, membrane transport and catalytic activity. Although liposomes are much simpler than cellular membranes, they are still challenging to study and a variety of complementary techniques are needed. In this review article, we consider several currently used analytical methods for spectroscopic measurements of unilamellar liposomes and their interaction with proteins and peptides. Among the variety of spectroscopic techniques seeing increasing application, we have chosen to discuss: fluorescence based techniques such as FRET (fluorescence resonance energy transfer) and FRAP (fluorescence recovery after photobleaching), that are used to identify localisation and dynamics of molecules in the membrane; circular dichroism (CD) and linear dichroism (LD) for conformational and orientation changes of proteins on membrane binding; and SERS (Surface Enhanced Raman Spectroscopy) as a rapidly developing ultrasensitive technique for site-selective molecular characterisation. The review contains brief theoretical basics of the listed techniques and recent examples of their successful applications for membrane studies.

Introduction

Membrane proteins are estimated to comprise up to 30% of all protein types in biological systems [1]. However, this is not reflected in structural data repositories with membrane proteins typically being 1% of available types [2]. To bridge this inconsistency, methods that probe membrane proteins in environments that mimic a biological system are required.

Molecular spectroscopic methods involve measuring changes that occur when electromagnetic radiation (often generically referred to as light) interacts with a molecular system. The wavelength of light used ranges from radio waves to γ-rays, whilst species studied range in size from single molecules containing a few atoms to large molecular assemblies [3]. This review focuses on certain spectroscopic measurements of unilamellar liposomes — spherical model of membrane bilayer systems — with proteins or peptides on or in the membrane (Figure 1). Unilamellar liposomes [4] are artificial membrane system which mimic many properties of the biological system being composed of a single lipid bilayer, containing one or more types of lipids. Biomolecules can bind on the lipid surface or in the bilayer to enable us to study structure, kinetics, catalysis, membrane disruption, and membrane transport.

Received: 16 December 2020
Revised: 29 March 2021
Accepted: 1 April 2021

Version of Record published:
4 May 2021

Emerging Topics in Life Sciences (2021) **5** 61–75
https://doi.org/10.1042/ETLS20200354

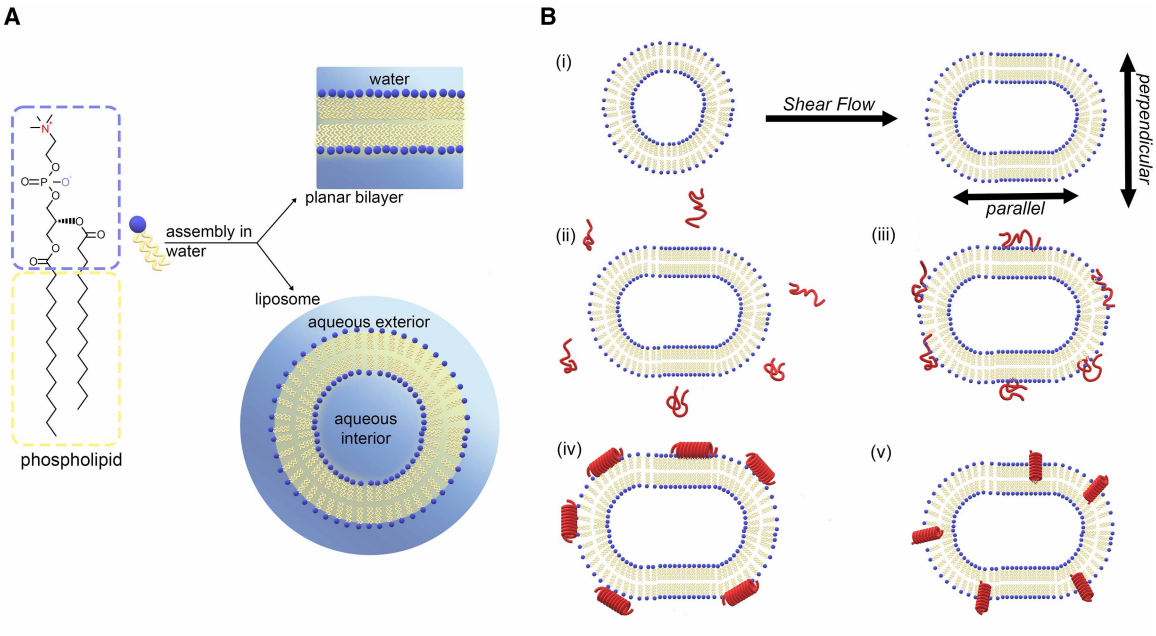

Figure 1. Schematic representation of the liposomes.

(**A**) Liposomal lipid bilayer. (**B**) (i) Liposome deformation under shear flow. (ii)–(v) Spherical model of membrane bilayer systems — with proteins or peptides on or in the membrane: unfolded peptides outside the liposome, unfolded peptides on the surface of the liposome, folded peptides on the surface of the liposome, and folded peptides in the liposomal membrane.

The first questions usually asked about protein–membrane interactions are:

(i) has the protein bound to (on or in) the membrane?
(ii) if so, what binding geometry has the protein adopted?
(iii) has the interaction affected the protein or the membrane?

We can address aspects of these questions by utilising liposomes, made with well-defined lipid compositions, that are suspended in aqueous (usually buffered) solutions. Liposomes are typically characterised by their size: small liposomes range up to ∼100 nm, large liposomes are deemed to be 100–1000 nm, and giant liposomes are anything that exceeds these sizes [4]. By using liposomes, we avoid the complexity of a multicomponent real biological membrane while avoiding the misleading results that follow from a sample being dehydrated following deposition onto a surface [5].

Rather simplistically, we can summarise the applications of different spectroscopies as follows. Fluorescence spectroscopy can be used to see whether environments around intrinsic and extrinsic fluorophores have changed. With targeted labelling, fluorescence can indicate the depth of a protein in the membrane, as well as giving an indication of protein and lipid dynamics [6]. Circular dichroism (CD) spectroscopy quickly indicates whether a peptide or protein has changed conformation [7] and linear dichroism (LD) [8] can be used to determine the orientation of protein secondary structures with respect to the membrane normal. These spectroscopies are usually implemented with UV-visible light. The lipids are only apparent with UV techniques due to the light scattering that occurs when the lipids assembled into particles (liposomes) comparable in size to the wavelength of the light. To probe the lipids *per se*, vibrational spectroscopies such as infra-red absorbance (IR) and Raman may be employed. Our focus here is on Surface Enhanced Raman Spectroscopy (SERS) [9]. Membrane–protein spectroscopy experiments are prone to artefacts resulting from light scattering and absorption flattening so care must be taken. The scattering component of any spectroscopy measurement can be minimised by reducing the distance from the sample to the detector. However, scattering is seldom completely removed and care must be taken while undertaking a baseline correction, especially when the spectroscopic signals are small relative to the scattering. It should be noted that scattering signals do contain useful information [10], but with liposomes little work has been done to develop methods to extract it [11].

Emerging Topics in Life Sciences (2021) **5** 61–75
https://doi.org/10.1042/ETLS20200354

Fluorescence of membrane-bound peptides

Fluorescence spectroscopy involves measuring the amount and wavelength of light emitted after molecules have been excited to a higher energy level. There is a wide range of fluorescence techniques, but our focus is on ones that are most useful for membrane–protein systems [6]. Nearly all fluorescence occurs from the lowest electronic excited state, as solution-phase molecules usually find non-radiative pathways to lose the energy to get back to that level. Fluorescent chromophores then return to the ground state through the emission of light. The frequency of the emitted light is typically less than that required to excite the molecules as illustrated in Figure 2A. For biomolecules we usually choose an excitation wavelength and scan over the emission wavelength, because scanning the excitation wavelength produces a spectrum similar to its absorbance spectrum (though usually with the longest wavelength band enhanced in intensity relative to shorter wavelength bands). The simplest application of protein emission fluorescence is to monitor any shift of tryptophan fluorescence when a protein or peptide is added to a solution of liposomes. A hydrophobic environment causes the tryptophan fluorescence maximum to move towards 330 nm from values as high as 350 nm. The usual excitation wavelength is 280 nm, but this induces fluorescence from both tyrosines and tryptophans. The former is not environment sensitive, so exciting at 295 nm selectively for tryptophan gives clearer information about its surface environment. An example of the fluorescence of gramicidin A's tryptophans in water and in a membrane is shown in Figure 2B. It should be noted that merely dipping the tryptophans into the headgroup region of the bilayer is sufficient to move the fluorescence to 325 nm, and that no further change is observed when the backbone of gramicidin fold and inserts (see below).

FRET (fluorescence resonance energy transfer) and FRAP (fluorescence recovery after photobleaching) both provide useful information about protein–lipid systems. FRET involves illuminating a fluorophore and measuring the resulting emission from another (donor and acceptor in Figure 3) — so they have to be close enough to transfer energy, with the intensity following Förster's [13, 14]. FRET is especially useful in estimating intramolecular distances and dynamic conformational changes perhaps as a function of property change measurements (e.g. a pH change) [15]. The technique has limitations connected with the need for an absorbing chromophore/accepting fluorophore pair and low signal-to-noise ratio. These issues can be overcome in most cases [16].

For example, Gorbenko et al. [17] used FRET assay to estimate the penetration depth of 1–83 N-terminal fragment of the protein apoA-I (A83) into the lipid bilayer. The FRET efficiency between donor (tryptophan) and acceptor (4′-N,N-dimethylamino-4 methylacryloylamino chalcone, DMC) was determined. The results helped to estimate the penetration depth of apoA-I variants into the membrane, which proved to depend on the cholesterol concentration. The work also illustrates the value of molecular dynamics simulations to interpret fluorescence data. The same principle was used by Elderdfi and Sikorsk [18] to find the equilibrium dissociation constant

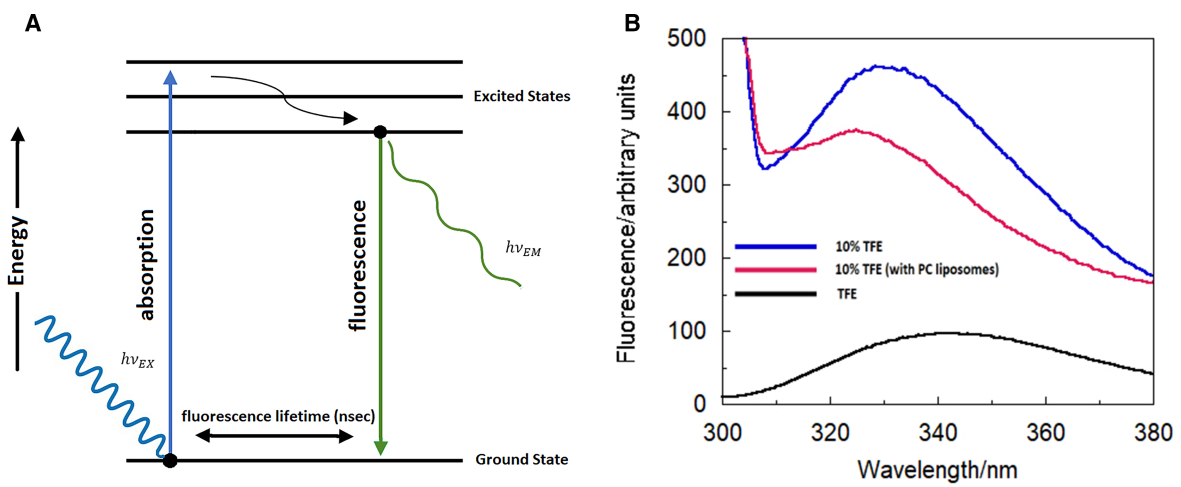

Figure 2. Fluorescence spectroscopy.

(**A**) Schematic energy level diagram for fluorescence spectroscopy — Jablonski diagram (omitting vibrational energy levels).

(**B**) Fluorescence of gramicidin A (a linear pentadecapeptide from Bacillus brevis with alternating D and L amino acids of which 4 are tryptophans) in TFE (black), 10% TFE (blue) and 10% TFE in the presence of PC liposomes (red) [12].

Emerging Topics in Life Sciences (2021) **5** 61–75
https://doi.org/10.1042/ETLS20200354

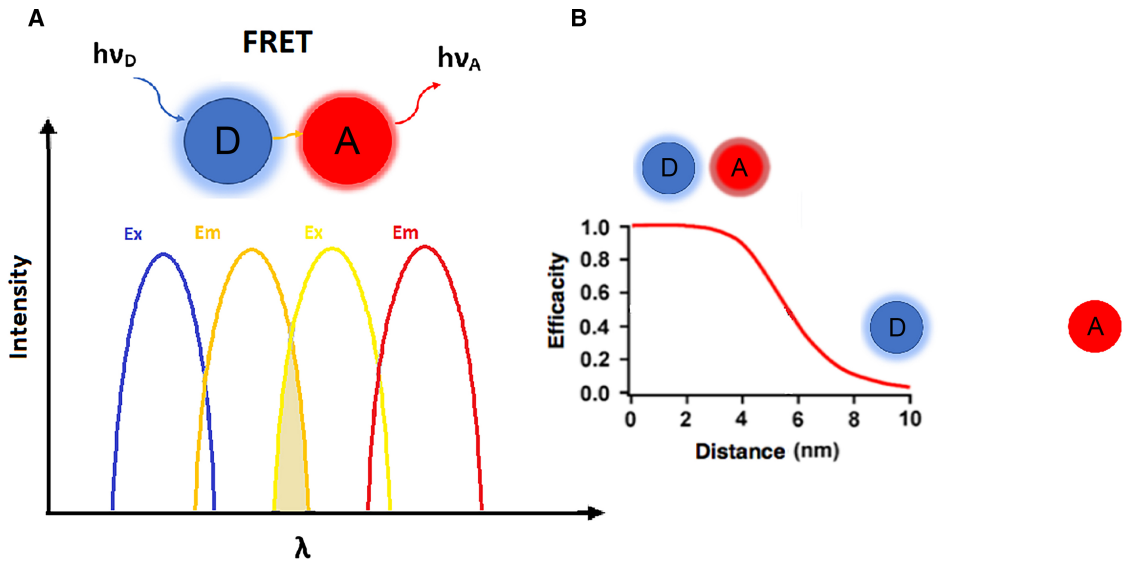

Figure 3. Fluorescence resonance energy transfer.

(**A**) Principle of FRET: transfer of excitation energy of a donor (D) fluorophore to a nearby acceptor (A) fluorophore in spectral overlap. (**B**) Correlation between the FRET efficiency and the distance between the fluorophores.

value of the binding affinity of membrane palmitoylated protein-1 (MPP1) with DOPC/SM/CH liposomes. The fluorescence signal of the dansyl labelled liposomes (acceptor) increased in the presence of tryptophan residues of protein MPP1 (donor). Membrane–protein interactions have also been studied by Lasitza-Male et al. [19] by probing the dynamics of DtpA protein (a proton-transporter) in various lipid environments (Figure 4).

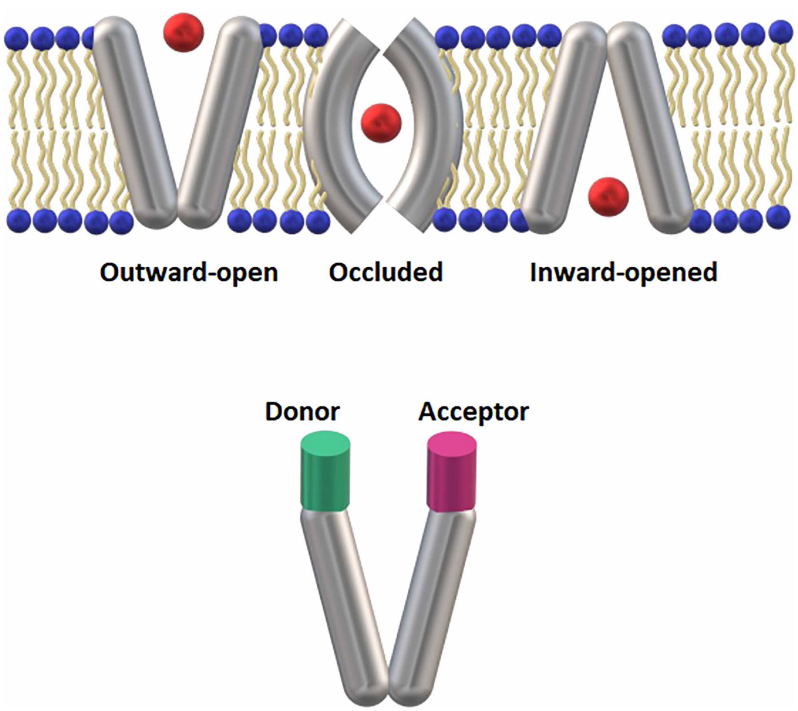

Figure 4. Schematics of the functionality of transport via DtpA, labelled for a FRET assay.

The top image demonstrates the different structural models of the DtpA conformers (grey) for the substrate (red) transport. The bottom image demonstrates the localisation of FRET dyes (green and pink) on the DtpA (grey).

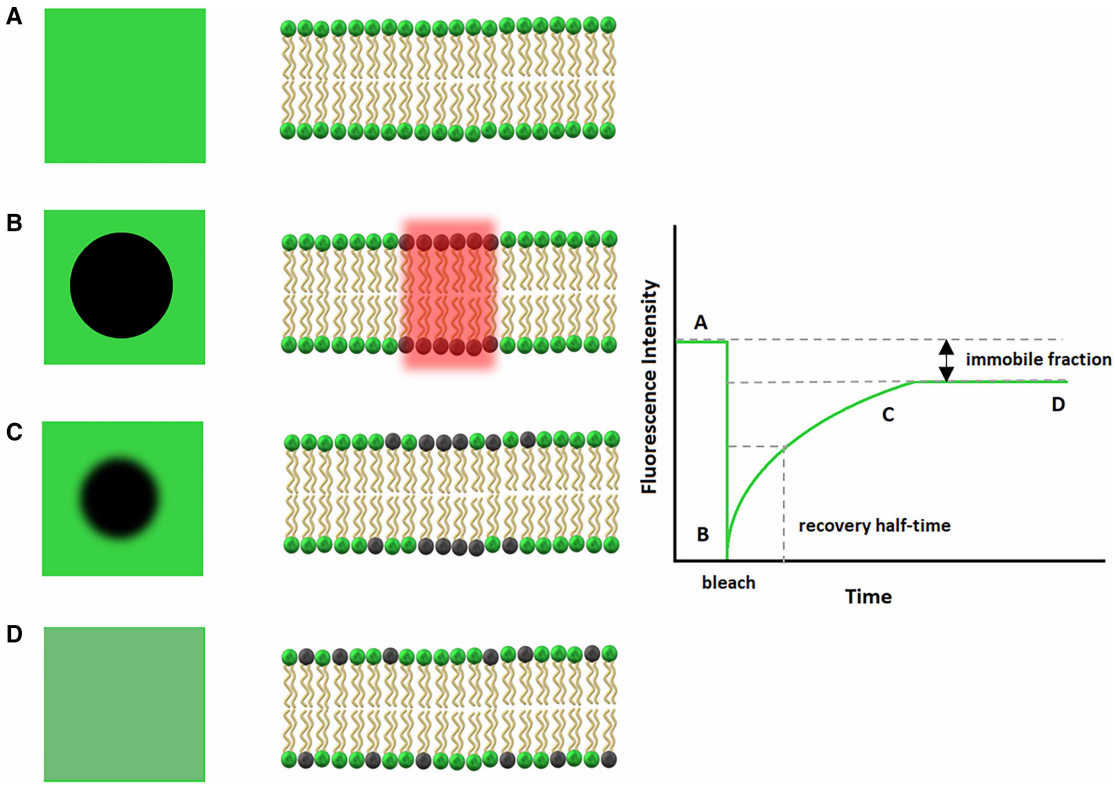

Figure 5. Schematic illustration of FRAP where a specific area of a lipid bilayer is photobleached by intense laser light, removing fluorescence from this area.

(**A**) the fluorescent region of the lipid bilayer, (**B**) bleaching of the monitored region by laser, (**C**) diffusion of the molecules, (**D**) recovery of the bleached region.

The existence of various lipid fluorophores allows the use of the FRET techique to study lipid layer dynamics. For instance, the phase separation behaviour of a lipid bilayer containing the photopolymerizable, diacetylene lipid (DiynePC) was investigated by Okuno et al. [20] using a FRET assay with NBD-PE and Rhod-PE as a pair of fluorescent lipids, distributed in the DOPC-rich phase in lipid bilayers. When the phase separation triggered by temperature change occurred between DiynePC and DOPC, fluorophores became concentrated in DOPC domains and FRET efficiency increased.

FRAP (fluorescence recovery after photobleaching) is less relevant in spectroscopy than in microscopy. In FRAP, the monitored fluorescent region is bleached by a high-intensity laser. The bleached region then recovers due to the diffusion of molecules. The recovery of fluorescence intensity is monitored and recorded into a recovery curve (Figure 5). The plotted data contains the information required to calculate lateral diffusion coefficients, which are in turn used in membrane dynamics study. FRAP has been applied for comparative study of new types of liposomes [21–23], fluidity of the lipid bilayers [24, 25] and proteins' dynamics in the membrane [26, 27]. The main limitations of FRAP are photoswitching of analyte chemical or structural analytes and localised heating by the laser [28] which can change the sample.

Circular dichroism

Membrane-binding peptides and membrane-binding domains of proteins frequently change structure when they move from hydrophilic to hydrophobic environments. Far UV CD spectra take only a few minutes to collect and immediately indicate whether a peptide is unfolded or helical (Figure 6A). CD is the differential absorbance of left and right circularly polarised light:

$$\mathrm{CD} = A_l - A_r = (\varepsilon_l - \varepsilon_r)CL \qquad (1)$$

Emerging Topics in Life Sciences (2021) **5** 61–75
https://doi.org/10.1042/ETLS20200354

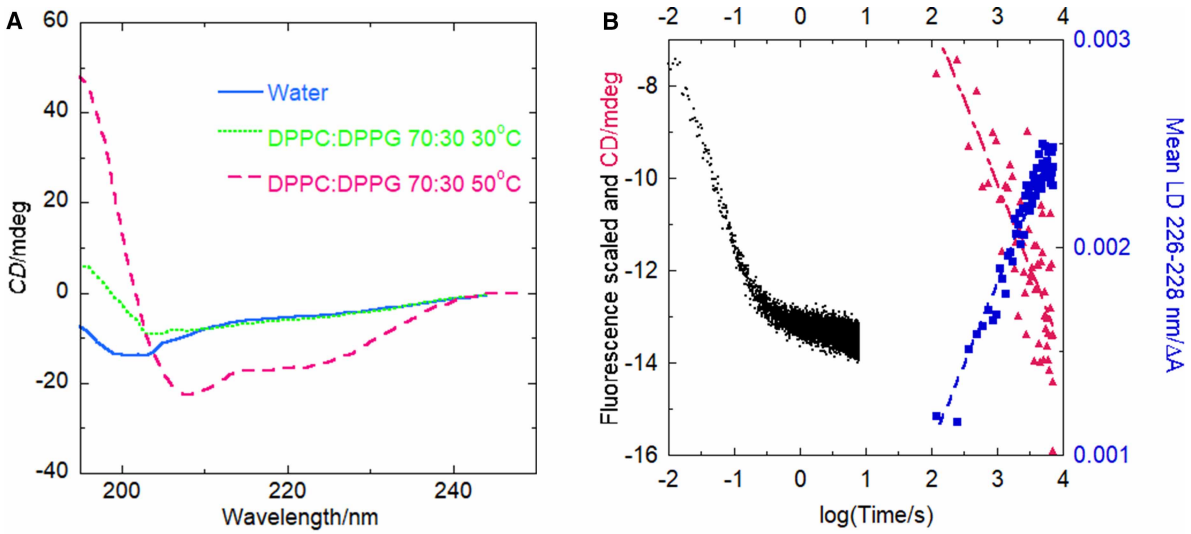

Figure 6. Examples of CD spectra indicating the peptide conformation state.

(**A**) CD spectrum of Aurein 2.5 (0.1 mg/ml) in water (solid blue line) showing a small negative CD signal at 200 nm characteristic of an unfolded peptide, in a mixed lipid in a gel phase showing a partially folded peptide (dotten green line), and in a mixed lipid in a fluid phase showing a spectrum characteristic of a helical peptide in a hydrophobic environment (dashed red line with 208 nm more intense than 222 nm) [31]. (**B**) Overlay of fluorescence (excitation at 292 nm emission >320 nm), CD, and LD of gramicidin A (50 μg/ml) as a function of time with phosphatidyl choline liposomes (1.8 mg.ml) in 10% v/v TFE. Fluorescence pathlength 0.8 mm, CD and LD pathlengths 0.5 mm. Note the time axis is logarithmic so fluorescence-detected changes occur within 100 ms whereas CD and LD changes occur on the same but much longer timescale with almost nothing happening for the first few seconds (data not shown) [12].

where A denotes absorbance, l is left (circularly polarised light), r is right, C is concentration and L is a path length. Electronic CD is uniquely sensitive to the net helical change in electron configuration due to an electronic transition. Protein CD spectra in near-UV region indicate when the environment of aromatic residues has changed [29, 30]. Protein backbone CD (~180–250 nm) spectra indicate when there has been a change in the secondary structure and can be used to measure the kinetics of folding (which may be initiated upon membrane insertion and thus is an indirect measure of insertion or orientation) in a membrane (Figure 6B). It should be noted that fluorescence suggests the insertion is much faster than the folding. However, the linear dichroism (see below) shows the reorientation of the peptide occurs on the CD timescale. Thus, fluorescence is showing when tryptophans dip into the membrane, CD indicates when the peptide folds, which in this case is coincident with insertion [12].

CD, to a good approximation, may be deemed to be the sum of the signals of all the component parts, and there are several structure-fitting methods which can be used to give a reasonable estimate of the number of residues that are in different secondary structure motifs [32–40]. Most approaches select members of a reference set of protein CD spectra that most closely resemble an unknown text spectrum and then determine the secondary structure context of the unknown protein from a weighted sum of the secondary structure percentages of the best matching members of the reference spectra [36, 41–44]. The website DichroWeb enables registered users to apply SELCON, CONTIN, CDSSTR and K2D analysis programs with a range of reference sets to do this [45, 46].

When one is considering the CD of proteins in membrane environments [47, 48], it is important to recognise that the wavelengths of transitions and shapes of spectra may move relative to their positions in aqueous solution in part due to the dielectric constants of the medium and in part because secondary structure motifs in membranes tend to be longer than in globular proteins, thus having fewer residue in the less tightly held ends of e.g. helices. Red shifts of n-π^* transitions (which occur at ~220 nm in proteins) in hydrophobic environments are well-established, with the converse operative to a lesser extent for π-π^* transitions (190–210 nm in proteins). Such effects are sometimes observed for membrane proteins [7]. It is almost always the case that the 208 nm signal for a helical membrane protein/peptide is greater than its 222 nm signal [49].

It is widely accepted that CD spectra down to 190 nm contain three independent pieces of information whereas data down into the vacuum UV region (say 175 nm) can provide more information [50]. However, we have recently shown, using Bayesian inference, that it is not possible to identify more than 3 distinct secondary structure classes from CD spectra above 175 nm, though more data do slightly improve the quality of the helix and sheet estimates [51]. The quality of the reference set has more impact on the reliability of a secondary structure estimate from CD. Therefore it is important that any reference set used for membrane protein structure fitting includes proteins in similar environments [52]. We have also shown the importance of being able to interrogate which members of a reference set are being selected, especially for the situation where random coil, polyproline II, and so-called β_{II} structures are present as they are structurally different but provide have essentially identical far UV CD spectra. So, if a best matching spectrum has been identified as having β_{II} structure (e.g. chymotrypsin, elastase, chymotrypsinogen, carbonic anhydrase [53] or indeed the β-structure of lysozyme [54]) care must be taken when attributing the secondary structure of an unknown to β, polyproline or random coil. For this purpose, our own self-organising map fitting approach SOMSpec is preferred because its output includes the map from the trained reference set and the position on the map of the unknown [44, 55].

Linear dichroism

Linear dichroism (LD) is the differential absorbance of light polarised parallel and perpendicular to an orientation direction, so any oriented sample will show a signal in its electronic as well as vibrational transitions. Liposomes and anything bound to them may be oriented in aqueous solution by subjecting them to shear flow which distorts the liposome into some form of ellipsoid [11, 56–58]. A Couette cell (Figure 7A) has the advantage of providing shear flow without losing the sample and, with a capillary Couette cell, volumes can go down as low as 25 μl [59, 60]. Other designs to give shear orientation are also possible [61]. Anything in the solution that is not bound to the liposome is not oriented and so gives no LD signal — though they do contribute to the overall absorbance which affects the reduced LD (LD divided by absorbance) and thence the data analysis. The equation for the LD of liposome-systems is slightly different from that used for molecules such as DNA and fibrous proteins as the unique molecular axis is parallel to the lipids and perpendicular to the liposome surface [11, 56–58]:

$$LD = A_{//} - A_{\perp} \tag{2}$$

and the reduced LD for liposomes is:

$$LD^r = \frac{LD}{A_{iso}} = \frac{3S}{4}(1 - 3\cos^2\beta) \tag{3}$$

where β is the angle the transition moment of interest makes with the membrane normal and S is orientation factor S (which is 1 for perfect orientation and 0 for random samples). S is typically of the order of 0.03 for liposomes of 100 nm size [11, 62]. This means [11, 63] that the long axis to short axis aspect ratio is ∼2.0. The LD of something bound on or in a liposome is therefore positive if the transition of interest (the electronic motion or vibration) is more parallel to the membrane surface than perpendicular to it (54.7° is the point where it swaps from positive to negative) and negative when it is more perpendicular to it.

In general, the key to interpreting a liposome flow LD spectrum is to know the transition polarisations of the molecules that are bound to the membrane [56]. Some key chromophores for peptides and proteins are illustrated in Figure 7B. The α-helix shows a clear n-π^* transition at ∼220 nm in both CD and LD that is polarized across the short axis of the helix. So, if a helical peptide is inserted into the membrane parallel to the lipids, 220 nm has a positive LD signal. The other two transitions which can be access for an α-helix are two perpendicular exciton components of the first π-π^* transition which occur at ∼210 nm and 190 nm. When inserted into the membrane, the 210 nm signal is expected to be negative, however, in practice looks like a positive minimum between two larger positive signals (Figure 7C). A β-sheet by way of contrast shows little net LD at 220 nm due to two cancelling transition components and the π-π^* transition is a single band a bit below 200 nm.

Liposome flow LD experiments can be used to follow the kinetics of membrane binding if it happens slowly enough. Normal Couette flow cells have a deadtime of ∼30 s (the cell assembly time). Rapid injection [64] and channel flow systems [65] can be used to reduce the dead time to 500 μs and 25 μs respectively, though with the penalty of more sample and worse signal-to-noise relative to Couette flow.

Emerging Topics in Life Sciences (2021) **5** 61–75
https://doi.org/10.1042/ETLS20200354

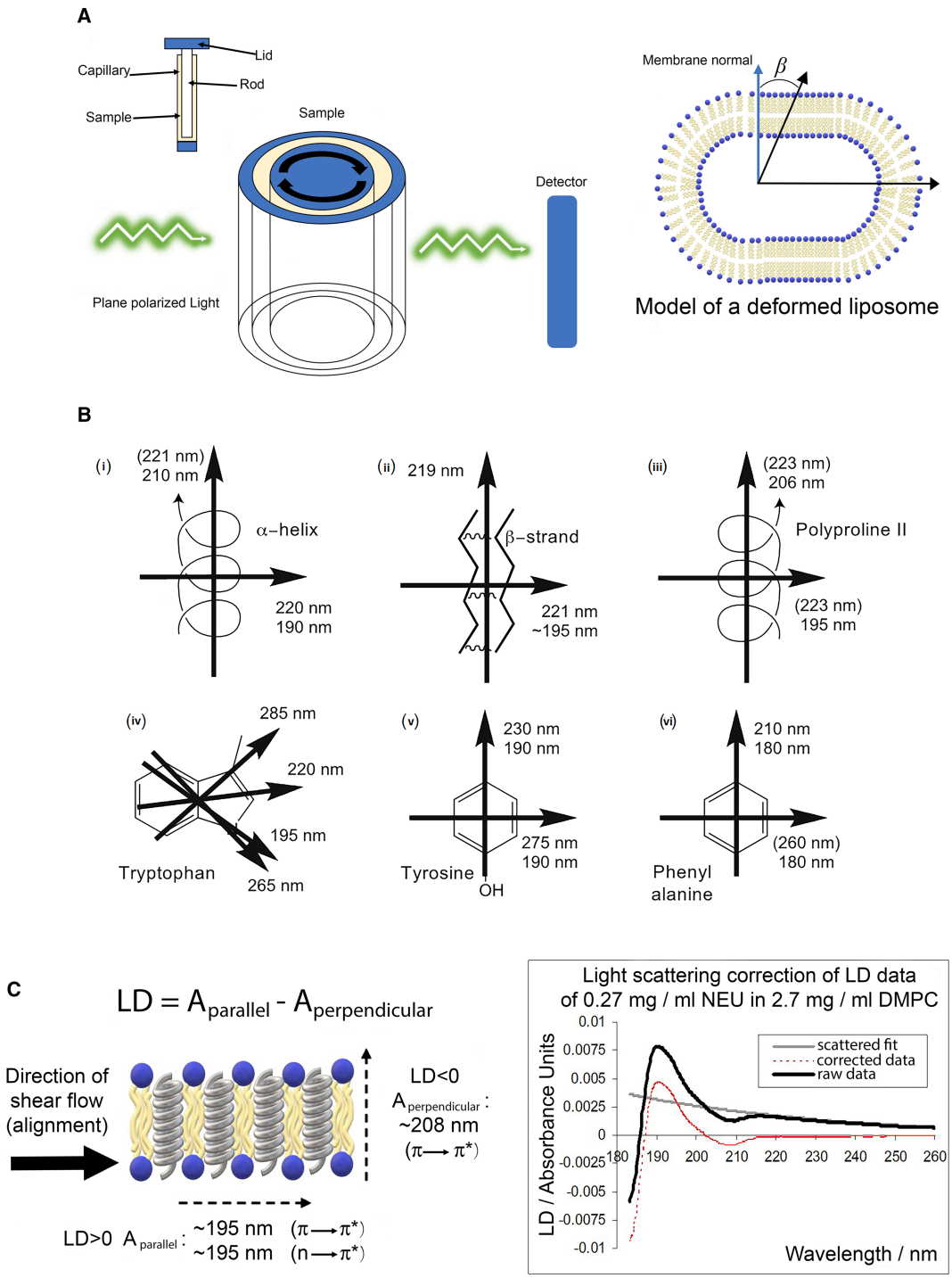

Figure 7. Linear dichroism spectroscopy.

(**A**) Couette flow cell and schematic of a flow-oriented liposome. (**B**)Transition polarisations in some key chromophores: (i) α-helix, (ii) β-sheet, (iii) polyproline type II, (iv) tryptophan, (v) tyrosine, and (vi) phenyl alanine. Thick arrows indicate transition moment polarizations. Approximate wavelength maxima of the transitions is indicated near the arrows. Wavelengths in brackets indicate the weak intensity of transition at given value. (**C**) LD of a helical peptide NEU [55] at a peptide concentration of 0.27 mg/ml and a lipid concentration of 2.7 mg/ml. The LD data were acquired using a Couette cell of 0.5 mm pathlength rotating at 3 V. The negative 208 nm signal indicates the helices are inserted parallel to the lipids, perpendicular to the membrane surface, so the helix long axis is perpendicular to the flow direction.

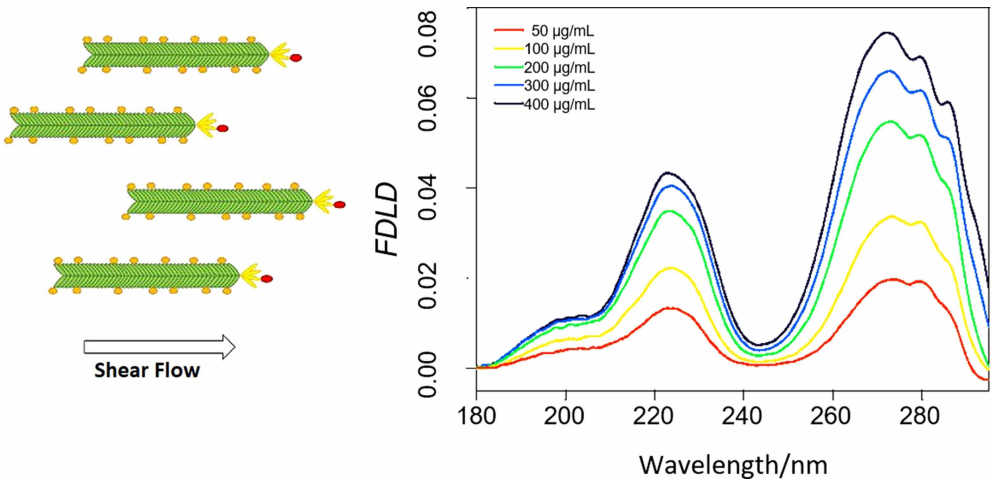

Figure 8. FDLD of M13 bacteriophage aligned in Couette flow (0.5 mm path length) (bacteriophages depicted on the left and FDLD spectra on the right) [69] showing the relatively larger magnitude signals for the lowest electronic state of tryptophans as found in standard fluorescence measurements.

Data were collected with a Jasco J-815 spectropolarimeter adapted for LD with Semrock 300 nm long-pass edge filter inserted before the detector to block transmitted incident light. The signatures of tryptophan's indole chromophore ^1L_a and ^1L_b bands are apparent in the 280 nm region of the spectra. The signals that dominate the LD spectra, namely DNA at 255 nm and protein backbone signals at 210 and 190 nm [70], are absent from the FDLD which only detects fluorophores.

One of the challenges of liposome LD spectroscopy, as discussed above, is that overlaid on any liposome LD spectrum one collects is a scattering or turbidity LD, as the unilamellar lipid vesicles typically used in LD experiments are of the order of the wavelength of light. Since a spectrometer detector simply counts the photons that are incident onto it, photons that do not arrive due to scattering are not differentiated from those missing due to absorbance. The spectrum in Figure 7C shows the original liposome flow *LD* spectrum of a helical peptide before and after correction for scattering [66].

Fluorescence detected linear dichroism

Hybrid techniques are invariably more complex to implement than either of their components but are richer in information content. Fluorescence-detected LD (FDLD) is one such example where the sensitivity and selectivity of fluorescence can be used to probe the orientation of selected chromophores in a sample (Figure 8). By inserting high quality long-pass cut-off filters into a standard CD machine that has been adapted for LD one can measure FDLD [67, 68]. It should be noted that some features of more modern instruments designed to ensure users collect good CD data may need to be disabled.

Raman

Vibrational spectroscopies give information about bonds, and hence conformations of molecules as a function of their environments [39]. For liposome-protein systems vibrational spectroscopies are particularly attractive as means of accessing the lipid bonds which are invisible in electronic spectroscopy. Infra-red absorbance (IR) is most widely used in general applications. However, most protein–lipid work in the literature is for samples deposited on surfaces rather than in solution. In addition, deuterated samples are often preferred due to overlap of water and protein amide I signals [71–73]. Thus, although there is great potential for membrane/protein IR, here we focus on how Raman spectroscopy can be used to give information to understand and control cellular processes.

Raman has the advantage over IR, whereby H_2O scattering is comparatively weak so that the signals of analytes can be extracted from higher concentration solutions. However, Raman scattering by its nature — it is a second-order process [74] — is generally weak with poor signal to noise ratios. Signals can be enhanced by Raman tags or 'reporter' molecules which are bound to targeted compartments of the membrane to generate enhanced Raman signals. Alternatively, so-called label-free 'surface-enhanced' Raman spectroscopy (SERS), which is based on the use of plasmonic nanomaterials to obtain enhanced Raman signals, may be used [9, 75]. There is a consensus in modern scientific society on the mechanisms underlying the enhancement of the

Emerging Topics in Life Sciences (2021) **5** 61–75
https://doi.org/10.1042/ETLS20200354

Raman signal (enhancement factor or EF). The EF builds on the combination of electromagnetic enhancement that occurs due to plasmon resonance on the metal particles, and chemical enhancement caused by the (partial) transfer of electrons between metal particles and molecules near their surface. As illustrated in Figure 9, label-free SERS can enhance Raman signals by at least two orders of magnitude, enabling single molecule SERS in some cases [76].

The incubation of liposomes with metal nanoparticles [77–80] is simple and does not require much preparation, with quality of data largely being dependent on the quality of the nanoparticles. The method has proved to be useful for lipid membrane analysis [81]. However, the descriptor, e.g. 'gold nanoparticle' is misleading as the metallic centre invariably has another ion, such as citrate, or, any other purpose-specific functionalisation [82] on the surface of the metal core. The surface-functionalisation [83] as well as particle size [84] and shape [85] influence the membrane-particle interaction and should be considered. If a membrane protein is being studied by SERS with metal nanoparticles it is advisable to check whether the particle–protein interaction is changing the secondary structure of the protein. CD is usually the simplest option.

Examples of how SERS can be used with liposomes are provided by Faried et al. [77] who performed location-specific analysis on the DMPG membranes (Figure 10) using 1-octanethiol capped gold nanoparticles of sizes 100 nm and 5 nm. The larger 100 nm particles preferentially enhanced signals from the surface region of the monolayer (e.g. C = O), while 5 nm particles became embedded inside the DMPG bilayer, enhancing the hydrophobic region (e.g. *trans* C–C signals and others in the fingerprint region (500–2000 cm^{-1}) and C–H stretching regions (2700–3100 cm^{-1})). Small particles influenced the lipid fluidity and polarity of the membranes by weakening hydrophobic interactions between lipids' molecules. However, overall the effect was not significant and it was concluded that embedding of the particles into the lipid bilayer does not disturb the membrane properties, which is also supported by their previous observation for DOPC/CH liposomes [82].

Novel approaches to membrane (phosphatidylcholine, sphingomyelin, and cholesterol) characterisation with citrate-stabilised gold nanoparticles for SERS in tandem with cryogenic electron microscopy (cryo-EM) have also

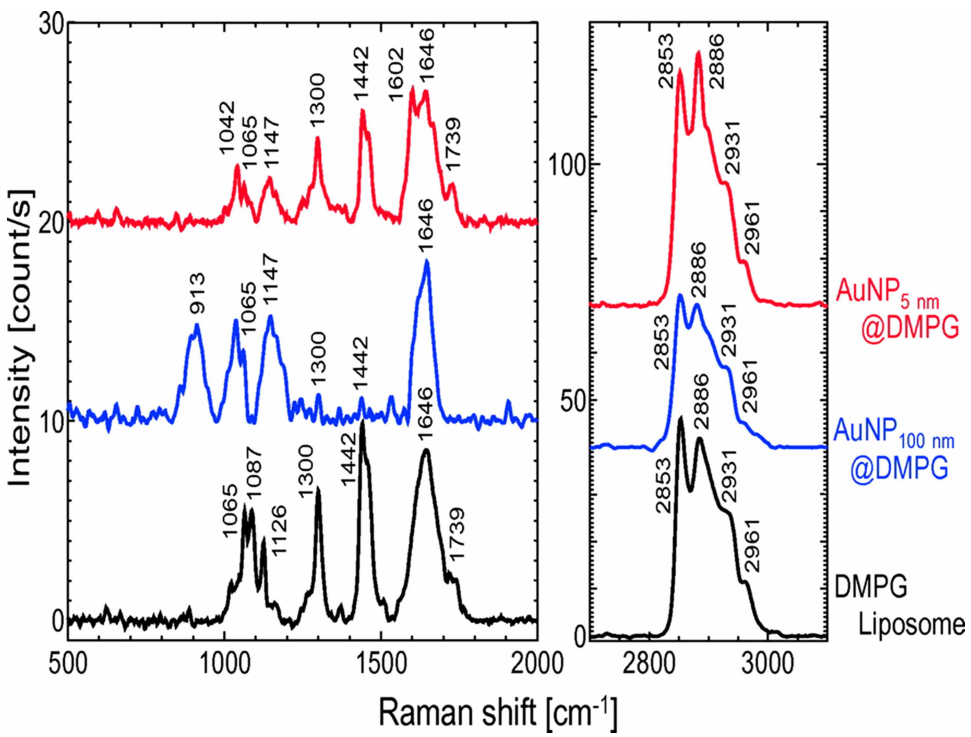

Figure 9. SERS vs Raman: Raman spectra of DMPG (1,2-dimyristoyl-sn-glycero-3-phosphoglycerol) liposome (black line, [DMPG] = 50 mM), $AuNP_{100nm}$@DMPG (blue line, [DMPG] = 1 mM), and $AuNP_{5nm}$@DMPG (red line, [DMPG] = 1 mM) (reproduced from [77] with permission).

Raman signal is enhanced by gold nanoparticles (1 mM concentration of DMPG is detected with the same signal intensity as 50 mM). Also, different size of nanoparticles enables to analyse various regions of the liposome.

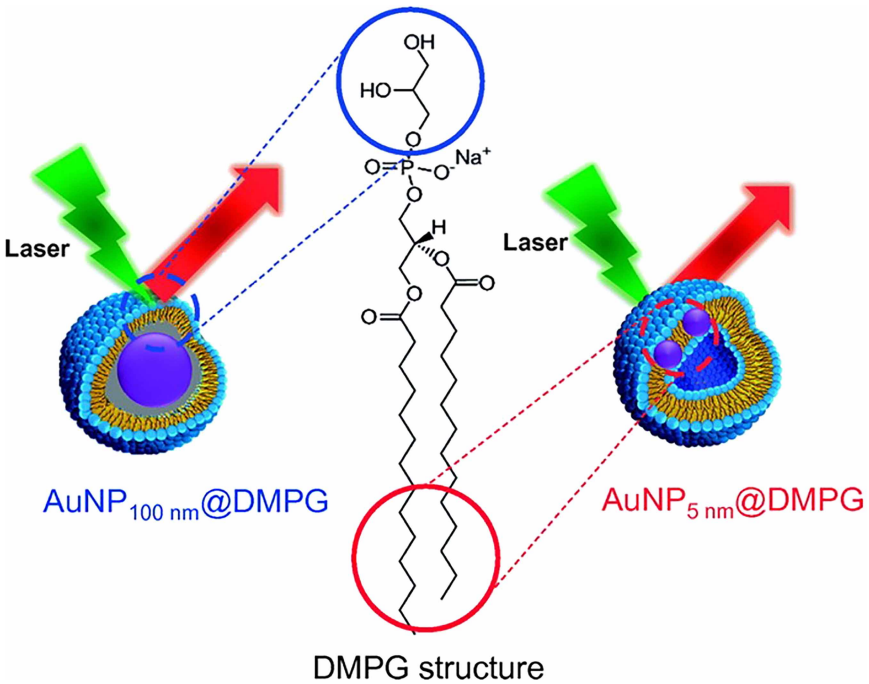

Figure 10. Gold nanoparticles in self-assembled lipid layers: large 100 nm gold nanoparticles covered with a DMPG monolayer and small 5 nm gold nanoparticles embedded inside the DMPG bilayer.
(Reproduced from [77] with permission).

been reported [80]. The EM images indicate nanoparticles of 30–50 nm in size and lead to the conclusion that the nanoparticles do not affect the membrane structure whereas higher concentrations of citrate do. Often, a principal component analysis is required to extract differences between preparations. For example, Delgado-Coello et al. [78] used 30 nm citrate-capped gold nanoparticles to characterise sphingomyelin/cholesterol-rich liposomes derived from cell membranes in order to describe the catalytic activity of a Ca^{2+}-ATPase calcium transporter as a function of the local lipid environment.

SERS gold nanoparticles also show potential to characterise not only artificial membrane systems but also the membranes of whole cells. Živanović et al. [86] studied (with 30 nm citrate capped gold particles) the distribution and interaction of the lipid molecules in parasitophorous vacuoles and the parasite of Leishmania-infected macrophage cells. Ramya et al. [79] were able to clearly distinguish lipids from other macromolecules including proteins, carbohydrates, and photosynthetic pigments via SERS (with 40 nm citrate capped gold particles) in *Scenedesmus quadricauda* CASA-CC202 under nitrogen starved condition and different pH.

Overall, SERS is a powerful technique for biomolecule characterisation. The different approaches and methodologies under this tool allow selective, dynamic, and site-specific study of the membrane compartments and processes. SERS can significantly enhance signals thus enabling very small amount of sample to be studied. Label-free SERS with gold nanoparticles is a relatively simple approach to obtain Raman signal of the membrane lipids and proteins. By tuning particle properties such as size, capping agent and shape, different sites can be targeted. It can be used in various applications including the monitoring of self-assembled lipids monolayers and characterisation of the whole cell membrane.

Summary

- Roughly 30% of all protein types in biological systems are membrane proteins. However, this is not representative with membrane protein being 1% of available types in our protein data bank. To bridge this inconsistency, methods that probe their structures in environments that mimic a biological system are required.

Emerging Topics in Life Sciences (2021) **5** 61–75
https://doi.org/10.1042/ETLS20200354

- Spectroscopic techniques, including absorbance, fluorescence, circular dichroism, linear dichroism, and surface enhanced Raman spectroscopy, can be applied to peptides and proteins bound to unilamellar liposome lipid bilayers to give structural information that can be combined to form a picture of the membrane–protein interaction.

- Combinations of techniques and their advancements are being developed to further enhance selectivity and sensitivity. Examples include surface enhanced Raman spectroscopy and fluorescence-detected linear dichroism.

Competing Interests

The authors declare that there are no competing interests associated with the manuscript.

Funding

A.T. acknowledges funding from Macquarie University Postgraduate Scholarship.

Open Access Statement

Open access for this article was enabled by the participation of Macquarie University in an all-inclusive *Read & Publish* pilot with Portland Press and the Biochemical Society under a transformative agreement with CAUL.

Author Contributions

The authors each wrote the first draft of half the text and half the diagrams and they wrote the final document together.

Abbreviations

apoA-I (A83), Apolipoprotein A1; ATP, Adenosine Triphosphate; AuNP, Gold Nanoparticle; CD, Circular Dichroism; CH, Cholesterol; DiynePC, Diacetylene Lipid; DMC, 4-Dimethylaminochalcone; DMPG, 1,2-Dimyristoyl-Sn-Glycero-3-Phospho-Rac-(1-Glycerol); DNA, Deoxyribonucleic Acid; DOPC, Dipalmitoyl Phosphatidylcholine; DtpA, diethylenetriaminepentaacetic acid; EF, Enhancement Factor; EM, Electron Microscopy; FDLD, Fluorescence Detected Linear Dichroism; FRAP, Fluorescence Recovery After Photobleaching; FRET, Fluorescence Resonance Energy Transfer; FTIR, Fourier-transform infrared spectroscopy; IR, Infra-Red; LD, Linear Dichroism; MPP1, Membrane Palmitoylated Protein-1; NBD-PE, Nitrobenzoxadiazole Labelled Lipid; NP, Nanoparticles; NP_{100}, 100 nm nanoparticle; NP_5, 5 nm nanoparticle; PE, Phosphatidylethanolamine; PS, Phosphatidylserine; Rhod-PE, Rhodamine Labelled Lipid; SERS, Surface Enhanced Raman Spectroscopy; SM, Sphingomyelin; TFE, Trifluoroethanl; UV, Ultra-Violet.

References

1 Almén, M.S., Nordström, K.J.V., Fredriksson, R. and Schiöth, H.B. (2009) Mapping the human membrane proteome: a majority of the human membrane proteins can be classified according to function and evolutionary origin. *BMC Biol.* **7**, 50 https://doi.org/10.1186/1741-7007-7-50

2 Almeida, J.G., Preto, A.J., Koukos, P.I., Bonvin, A.M.J.J. and Moreira, I.S. (2017) Membrane proteins structures: a review on computational modeling tools. *Biochim. Biophys. Acta Biomembranes* **1859**, 2021–2039 https://doi.org/10.1016/j.bbamem.2017.07.008

3 JC, D. (2017) *Advances in the Application of Spectroscopic Techniques in the Biofuel Area Over the Last Few Decades*, IntechOpen

4 Akbarzadeh, A., Rezaei-Sadabady, R., Davaran, S., Joo, S.W., Zarghami, N., Hanifehpour, Y. et al. (2013) Liposome: classification, preparation, and applications. *Nanoscale Res. Lett.* **8**, 102 https://doi.org/10.1186/1556-276X-8-102

5 Siontorou, C.G., Nikoleli, G.-P., Nikolelis, D.P. and Karapetis, S.K. (2017) Artificial lipid membranes: past, present, and future. *Membranes* **7**, 38 https://doi.org/10.3390/membranes7030038

6 Johnson, A.E. (2005) Fluorescence approaches for determining protein conformations, interactions and mechanisms at membranes. *Traffic* **6**, 1078–1092 https://doi.org/10.1111/j.1600-0854.2005.00340.x

7 Miles, A.J. and Wallace, B.A. (2016) Circular dichroism spectroscopy of membrane proteins. *Chem. Soc. Rev.* **45**, 4859–4872 https://doi.org/10.1039/C5CS00084J

8 Daviter, T., Chmel, N. and Rodger, A. (2013) Circular and linear dichroism spectroscopy for the study of protein–ligand interactions. *Methods Mol. Biol.* **1008**, 211–241 https://doi.org/10.1007/978-1-62703-398-5_8

9 Bruzas, I., Lum, W., Gorunmez, Z. and Sagle, L. (2018) Advances in surface-enhanced Raman spectroscopy (SERS) substrates for lipid and protein characterization: sensing and beyond. *Analyst* **143**, 3990–4008 https://doi.org/10.1039/C8AN00606G

10 Vermeer, L.S., Marquette, A., Schoup, M., Fenard, D., Galy, A. and Bechinger, B. (2016) Simultaneous analysis of secondary structure and light scattering from circular dichroism titrations: application to vectofusin-1. *Sci. Rep.* **6**, 39450 https://doi.org/10.1038/srep39450
11 Dorrington, G., Chmel, N.P., Norton, S.R., Wemyss, A.M., Lloyd, K., Praveen Amarasinghe, D. et al. (2018) Light scattering corrections to linear dichroism spectroscopy for liposomes in shear flow using calcein fluorescence and modified Rayleigh-Gans-Debye-Mie scattering. *Biophys. Rev.* **10**, 1385–1399 https://doi.org/10.1007/s12551-018-0458-8
12 Hicks, M., Damianoglou, A., Rodger, A. and Dafforn, T. (2008) Folding and membrane insertion of the pore-forming peptide gramicidin occur as a concerted process. *J. Mol. Biol.* **383**, 358–366 https://doi.org/10.1016/j.jmb.2008.07.091
13 Haas, E. (2012) Ensemble FRET methods in studies of intrinsically disordered proteins. *Methods Mol. Biol.* **895**, 467–498 https://doi.org/10.1007/978-1-61779-927-3_28
14 Deal, J., Pleshinger, D.J., Johnson, S.C., Leavesley, S.J. and Rich, T.C. (2020) Milestones in the development and implementation of FRET-based sensors of intracellular signals: A biological perspective of the history of FRET. *Cell. Signal.* **75**, 109769 https://doi.org/10.1016/j.cellsig.2020.109769
15 Liu, L., He, F., Yu, Y. and Wang, Y. (2020) Application of FRET biosensors in mechanobiology and mechanopharmacological screening. *Front. Bioeng. Biotechnol.* **8**, 595497 https://doi.org/10.3389/fbioe.2020.595497
16 Leavesley, S.J. and Rich, T.C. (2016) Overcoming limitations of FRET measurements. *Cytometry A* **89**, 325–327 https://doi.org/10.1002/cyto.a.22851
17 Gorbenko, G.P., Trusova, V., Mizuguchi, C. and Saito, H. (2018) Lipid bilayer interactions of amyloidogenic N-terminal fragment of apolipoprotein A-I probed by Förster resonance energy transfer and molecular dynamics simulations. *J. Fluoresc.* **28**, 1037–1047 https://doi.org/10.1007/s10895-018-2267-7
18 Elderdfi, M. and Sikorski, A.F. (2018) Interaction of membrane palmitoylated protein-1 with model lipid membranes. *Gen. Physiol. Biophys.* **37**, 603–617 https://doi.org/10.4149/gpb_2018029
19 Lasitza-Male, T., Bartels, K., Jungwirth, J., Wiggers, F., Rosenblum, G., Hofmann, H. et al. (2020) Membrane chemistry tunes the structure of a peptide transporter. *Angew. Chem. Int. Ed. Engl.* **59**, 19121–19128 https://doi.org/10.1002/anie.202008226
20 Okuno, K., Saeki, D. and Matsuyama, H. (2020) Phase separation behavior of binary mixture of photopolymerizable diacetylene and unsaturated phospholipids in liposomes. *Biochim. Biophys. Acta Biomembranes* **1862**, 183377 https://doi.org/10.1016/j.bbamem.2020.183377
21 Schaich, M., Sobota, D., Sleath, H., Cama, J. and Keyser, U.F. (2020) Characterization of lipid composition and diffusivity in OLA generated vesicles. *Biochim. Biophys. Acta Biomembranes* **1862**, 183359 https://doi.org/10.1016/j.bbamem.2020.183359
22 Urban, P., Pritzl, S.D., Ober, M.F., Dirscherl, C.F., Pernpeintner, C., Konrad, D.B. et al. (2020) A lipid photoswitch controls fluidity in supported bilayer membranes. *Langmuir* **36**, 2629–2634 https://doi.org/10.1021/acs.langmuir.9b02942
23 Sut, T.N., Park, S., Yoon, B.K., Jackman, J.A. and Cho, N.-J. (2020) Optimal formation of uniform-phase supported lipid bilayers from phospholipid–monoglyceride bicellar mixtures. *J. Ind. Eng. Chem.* **88**, 285–291 https://doi.org/10.1016/j.jiec.2020.04.026
24 Hernaiz-Llorens, M., Roselló-Busquets, C., Durisic, N., Filip, A., Ulloa, F., Martínez-Mármol, R. et al. (2021) Growth cone repulsion to Netrin-1 depends on lipid raft microdomains enriched in UNC5 receptors. *Cell. Mol. Life Sci.* **78**, 2797–2820 https://doi.org/10.1007/s00018-020-03663-z
25 Jordan, L.R., Blauch, M.E., Baxter, A.M., Cawley, J.L. and Wittenberg, N.J. (2019) Influence of brain gangliosides on the formation and properties of supported lipid bilayers. *Colloids Surf. B Biointerfaces* **183**, 110442 https://doi.org/10.1016/j.colsurfb.2019.110442
26 Mystek, P., Rysiewicz, B., Gregrowicz, J., Dziedzicka-Wasylewska, M. and Polit, A. (2019) Gγ and Gα identity dictate a G-protein heterotrimer plasma membrane targeting. *Cells* **8**, 1246 https://doi.org/10.3390/cells8101246
27 Saha, S., Anilkumar, A. and Mayor, S. (2015) GPI-anchored protein organization and dynamics at the cell surface. *J. Lipid Res.* **57**, 159–175 https://doi.org/10.1194/jlr.R062885
28 De Los Santos, C., Chang, C.-W., Mycek, M.-A. and Cardullo, R.A. (2015) FRAP, FLIM, and FRET: detection and analysis of cellular dynamics on a molecular scale using fluorescence microscopy. *Mol. Reprod. Dev.* **82**, 587–604 https://doi.org/10.1002/mrd.22501
29 Woody, R.W. (2007) Aromatic side-chain contributions to protein circular dichroism. In *Methods in Protein Structure and Stability Analysis* (Uversky, V. and Permyakov, E., eds), pp. 291–344, Nova Science Publishers Inc, New York
30 Woody, R.W. (1994) Contributions of tryptophan side chains to the far uv circular dichroism of proteins. *Eur. Biophys. J.* **23**, 253–262 https://doi.org/10.1007/BF00213575
31 Hicks, M.R.D., Olamoyesan, A. and Rodger, A. (2021) Flow linear dichroism of protein–membrane systems. In *Protein-ligand Interactions: Methods and Applications* (Daviter, T., Johnson, C., McLaughlin, S. and Williams, M., eds), Springer, US
32 Bromley, E.H.C., Channon, K.J., King, P.J.S., N. Mahmoud, Z.N., Banwell, E. F. Bulter, M.F. et al. (2010) The assembly pathway of a designed α-helical protein fiber. *Biophys. J.* **98**, 1668–1676 https://doi.org/10.1016/j.bpj.2009.12.4309
33 Ennaceur, S.M., Hicks, M.R., Pridmore, C.J., Dafforn, T.R., Rodger, A. and Sanderson, J.M. (2009) Peptide adsorption to lipid bilayers: slow rearrangement processes revealed by linear dichroism spectroscopy. *Biophys. J.* **96**, 1399–1407 https://doi.org/10.1016/j.bpj.2008.10.039
34 Bulheller, B.M., Rodger, A. and Hirst, J.D. (2007) Circular and linear dichroism of proteins. *Phys. Chem. Chem. Phys.* **9**, 2020–2035 https://doi.org/10.1039/b615870f
35 Woody, R.W. (2009) Circular dichroism spectrum of peptides in the poly(Pro)II conformation. *J. Am. Chem. Soc.* **131**, 8234–8245 https://doi.org/10.1021/ja901218m
36 Sreerama, N. and Woody, R.W. (2000) Estimation of protein secondary structure from circular dichroism spectra: comparison of CONTIN, SELCON, and CDSSTR methods with an expanded reference Set. *Analyt. Biochem.* **287**, 252–260 https://doi.org/10.1006/abio.2000.4880
37 Woody, R.W. (1994) Circular dichroism of peptides and proteins. In *Circular Dichroism Principles and Applications* (Nakanishi, K., Berova, N. and Woody, R.W., eds), VCH, New York
38 Johnson, W.C.J. and Tinoco, I.J. (1972) Circular dichroism of polypeptide solutions in the vacuum ultraviolet. *J. Am. Chem. Soc.* **94**, 4389–4390 https://doi.org/10.1021/ja00767a084
39 Jones, J.E., Diemer, V., Adam, C., Raftery, J., Ruscoe, R.E., Sengel, J.T. et al. (2016) Length-dependent formation of transmembrane pores by 310-helical α-aminoisobutyric acid foldamers. *J. Am. Chem. Soc.* **138**, 688–695 https://doi.org/10.1021/jacs.5b12057
40 Wallace, B.A. and Janes, R. (2009) *Modern Techniques for Circular Dichroism Spectroscopy*, IOS Press, Amsterdam

41 Johnson, W.J. (1988) Secondary structure of proteins through circular dichroism spectroscopy. *Ann. Rev. Biophys. Biophys. Chem.* **17**, 145–166 https://doi.org/10.1146/annurev.bb.17.060188.001045
42 Hennessey, J.P. and Johnson, W.C. (1981) Information content in the circular dichroism of proteins. *Biochemistry*, 1085–1094 https://doi.org/10.1021/bi00508a007
43 Sreerama, N. and Woody, R.W. (1993) A self-consistent method for the analysis of protein secondary structure from circular dichroism. *Analyt. Biochem.* **209**, 32–44 https://doi.org/10.1006/abio.1993.1079
44 Hall, V., Sklepari, M. and Rodger, A. (2014) Protein secondary structure prediction from circular dichroism spectra using a self-organizing map with concentration correction. *Chirality* **26**, 471–482 https://doi.org/10.1002/chir.22338
45 Whitmore, L., Woollett, B., Miles, A.J., Klose, D., Janes, R.W. and Wallace, B.A. (2011) PCDDB: the protein circular dichroism data bank, a repository for circular dichroism spectral and metadata. *Nucleic Acids Res.* **39**, D480–D486 https://doi.org/10.1093/nar/gkq1026
46 Whitmore, L. and Wallace, B.A. (2004) DICHROWEB: an online server for protein secondary structure analyses from circular dichroism specroscopic data. *Nucleic Acids Res.* **32**, W668–W673 https://doi.org/10.1093/nar/gkh371
47 Cascio, M. and Wallace, B.A. (1995) Effects of local environment on the circular dichroism spectra of polypeptides. *Anal. Biochem.* **227**, 90–100 https://doi.org/10.1006/abio.1995.1257
48 Chen, Y. and Wallace, B.A. (1997) Secondary solvent effects on the circular dichroism spectra of polypeptides in non-aqueous environments: influence of polarisation effects on the far ultraviolet spectra of alamethicin. *Biophys. Chem.* **65**, 65–74 https://doi.org/10.1016/S0301-4622(96)02225-9
49 Damianoglou, A., Rodger, A., Pridmore, C., Dafforn, T., Mosely, J., Sanderson, J. et al. (2010) The synergistic action of melittin and phospholipase A2 with lipid membranes: a development of linear dichroism for membrane-insertion kinetics. *Protein Pept. Lett.* **17**, 351–362 https://doi.org/10.2174/092986611009011351
50 Wallace, B.A. and Janes, R.W. (2001) Synchrotron radiation circular dichroism spectroscopy of proteins: secondary structure, fold recognition and structural genomics. *Curr. Opin. Chem. Biol.* **5**, 567–571 https://doi.org/10.1016/S1367-5931(00)00243-X
51 Spencer, S.E.F. and Rodger, A. (2021) Bayesian inference assessment of protein secondary structure analysis using circular dichroism data – how much structural information is contained in protein circular dichroism spectra? *Anal. Methods* **13**, 359–368 https://doi.org/10.1039/D0AY01645D
52 Abdul-Gader, A., Miles, A.J. and Wallace, B.A. (2011) A reference dataset for the analyses of membrane protein secondary structures and transmembrane residues using circular dichroism spectroscopy. *Bioinformatics* **27**, 1630–1636 https://doi.org/10.1093/bioinformatics/btr234
53 Sreerama, N. and Woody, R.W. (2003) Structural composition of beta I- and beta II-proteins. *Protein Sci.* **12**, 384–388 https://doi.org/10.1110/ps.0235003
54 Olamoyesan, A., Rodger, A. and Ang, D. (2021) Unpublished work
55 Hall, V., Nash, A. and Rodger, A. (2014) SSNN, a method for neural network protein secondary structure fitting using circular dichroism data. *Anal. Methods* **6**, 6721–6726 https://doi.org/10.1039/C3AY41831F
56 Nordén, B., Rodger, A. and Dafforn, T.R. (2010) *Linear Dichroism and Circular Dichroism: A Textbook on Polarized Spectroscopy*, Royal Society of Chemistry, Cambridge
57 Rodger, A., Rajendra, J., Marrington, R., Ardhammar, M., Nordén, B., Hirst, J.D. et al. (2002) Flow oriented linear dichroism to probe protein orientation in membrane environments. *Phys. Chem. Chem. Phys.* **4**, 4051–4057 https://doi.org/10.1039/B205080N
58 Ardhammar, M., Mikati, N. and Nordén, B. (1998) Chromophore orientation in liposome membranes probed with flow linear dichroism. *J. Am. Chem. Soc.* **120**, 9957–9958 https://doi.org/10.1021/ja981102g
59 Marrington, R., Dafforn, T.R., Halsall, D.J. and Rodger, A. (2004) Micro-volume couette flow sample orientation for absorbance and fluorescence linear dichroism. *Biophys. J.* **87**, 2002–2012 https://doi.org/10.1529/biophysj.103.035022
60 Marrington, R., Dafforn, T.R., Halsall, D.J., Hicks, M. and Rodger, A. (2005) Validation of new microvolume couette flow linear dichroism cells. *Analyst* **130**, 1608–1616 https://doi.org/10.1039/b506149k
61 Lundahl, P.J., Kitts, C.C. and Nordén, B. (2011) A new highly adaptable design of shear-flow device for orientation of macromolecules for linear dichroism (LD) measurement. *Analyst* **136**, 3303–3306 https://doi.org/10.1039/c0an00455c
62 Rajendra, J., Damianoglou, A., Hicks, M., Booth, P., Rodger, P. and Rodger, A. (2006) Quantitation of protein orientation in flow-oriented unilamellar liposomes by linear dichroism. *Chem. Phys.* **326**, 210–220 https://doi.org/10.1016/j.chemphys.2006.02.036
63 McLachlan, J., Smith, D.J., Chmel, N.P. and Rodger, A. (2013) Calculation of flow-induced orientation distributions for analysis of linear dichroism spectroscopy. *Soft Matter* **9**, 4977–4984 https://doi.org/10.1039/c3sm27419e
64 Hicks, M.R., Rodger, A., Lin, Y., Jones, N.C., Hoffmann, S.V. and Dafforn, T.R. (2012) Rapid injection linear dichroism for studying the kinetics of biological processes. *Anal. Chem.* **84**, 6561–6566 https://doi.org/10.1021/ac300842h
65 Cheng, X., Joseph, M.B., Covington, J.A., Dafforn, T.R., Hicks, M.R. and Rodger, A. (2012) Continuous-channel flow linear dichroism. *Anal. Methods* **4**, 3169–3173 https://doi.org/10.1039/c2ay25513h
66 Beevers, A.J., Damianoglou, A., Oates, J., Rodger, A. and Dixon, A.M. (2010) Sequence-Dependent oligomerization of the Neu transmembrane domain suggests inhibition of 'conformational switching' by an oncogenic mutant. *Biochemistry* **49**, 2811–2820 https://doi.org/10.1021/bi902087v
67 Wemyss, A.M., Chmel, N.P., Lobo, D.P., Sutherland, J.A., Dafforn, T.R. and Rodger, A. (2018) Fluorescence detected linear dichroism spectroscopy: a selective and sensitive probe for fluorophores in flow-oriented systems. *Chirality* **30**, 227–237 https://doi.org/10.1002/chir.22795
68 Wemyss, A.M., Razmkhah, K., Chmel, N.P. and Rodger, A. (2018) Fluorescence detected linear dichroism of small molecules oriented on polyethylene film. *Analyst* **143**, 5805–5811 https://doi.org/10.1039/C8AN01588K
69 Wemyss, A.M. (2017) *The Development of Experimental and Analytical Techniques for the Study of Aligned Fluorophores*, University of Warwick, Coventry
70 Clack, B.A. and Gray, D.M. (1989) A CD determination of the alpha-helix contents of the coat proteins of four filamentous bacteriophages: fd, IKe, Pf1, and Pf3. *Biopolymers* **28**, 1861–1873 https://doi.org/10.1002/bip.360281103
71 Jawurek, M., Dröden, J., Peter, B., Glaubitz, C. and Hauser, K. (2018) Lipid-induced dynamics of photoreceptors monitored by time-resolved step-scan FTIR spectroscopy. *Chem. Phys.* **512**, 53–61 https://doi.org/10.1016/j.chemphys.2018.04.010
72 Derenne, A., Claessens, T., Conus, C. and Goormaghtigh, E. (2013) Infrared Spectroscopy of Membrane Lipids BT. In *Encyclopedia of Biophysics* (Roberts, G.C.K., ed.), pp. 1074–1081, Springer Berlin Heidelberg, Berlin, Heidelberg

73 Hauser, K. (2013) Infrared Spectroscopy of Protein Folding, Misfolding and Aggregation BT. In *Encyclopedia of Biophysics* (Roberts, G.C.K., ed.), pp. 1089–1095, Springer Berlin Heidelberg, Berlin, Heidelberg
74 Colomban, P. and Gouadec, G. (2008) Raman Scattering: Theory and Elements of Raman Instrumentation. In *Raman Spectroscopy* (Amer, M.S., ed.), pp. 11–29, Wiley https://www.wiley.com/en-au/Raman+Spectroscopy+for+Soft+Matter+Applications-p-9780470453834
75 Chisanga, M., Muhamadali, H., Ellis, D.I. and Goodacre, R. (2019) Enhancing disease diagnosis: biomedical applications of surface-enhanced Raman scattering. *Appl. Sci.* **9**, 1163 https://doi.org/10.3390/app9061163
76 Langer, J., Jimenez de Aberasturi, D., Aizpurua, J., Alvarez-Puebla, R.A., Auguié, B., Baumberg, J.J., et al (2020) Present and future of surface-enhanced Raman scattering. *ACS Nano* **14**, 28–117 https://doi.org/10.1021/acsnano.9b04224
77 Faried, M., Ando, S., Suga, K., Okamoto, Y. and Umakoshi, H. (2020) Site specific analysis of anionic lipid by membrane surface-enhanced Raman spectroscopy with different sized gold nanoparticles. *Chem. Lett.* **49**, 1107–1110 https://doi.org/10.1246/cl.200389
78 Delgado-Coello, B., Montalvan-Sorrosa, D., Cruz-Rangel, A., Sosa-Garrocho, M., Hernández-Téllez, B., Macías-Silva, M. et al. (2017) Label-free surface-enhanced Raman spectroscopy of lipid-rafts from hepatocyte plasma membranes. *J. Raman Spectrosc.* **48**, 659–667 https://doi.org/10.1002/jrs.5101
79 Ramya, A.N., Ambily, P.S., Sujitha, B.S., Arumugam, M. and Maiti, K.K. (2017) Single cell lipid profiling of Scenedesmus quadricauda CASA-CC202 under nitrogen starved condition by surface enhanced Raman scattering (SERS) fingerprinting. *Algal Res.* **25**, 200–206 https://doi.org/10.1016/j.algal.2017.05.011
80 Živanović, V., Kochovski, Z., Arenz, C., Lu, Y. and Kneipp, J. (2018) SERS and cryo-EM directly reveal different liposome structures during interaction with gold nanoparticles. *J. Phys. Chem. Lett.* **9**, 6767–6772 https://doi.org/10.1021/acs.jpclett.8b03191
81 Suga, K., Yoshida, T., Ishii, H., Okamoto, Y., Nagao, D., Konno, M. et al. (2015) Membrane surface-Enhanced Raman spectroscopy for sensitive detection of molecular behavior of lipid assemblies. *Anal. Chem.* **87**, 4772–4780 https://doi.org/10.1021/ac5048532
82 Faried, M., Suga, K., Okamoto, Y., Shameli, K., Miyake, M. and Umakoshi, H. (2019) Membrane surface-enhanced Raman spectroscopy for cholesterol-modified lipid systems: effect of gold nanoparticle size. *ACS Omega* **4**, 13687–13695 https://doi.org/10.1021/acsomega.9b01073
83 Ding, H.M. and Ma, Y.Q. (2016) Design strategy of surface decoration for efficient delivery of nanoparticles by computer simulation. *Sci. Rep.* **6**, 26783 https://doi.org/10.1038/srep26783
84 Gupta, R. and Rai, B. (2017) Effect of size and surface charge of gold nanoparticles on their skin permeability: a molecular dynamics study. *Sci. Rep.* **7**, 45292 https://doi.org/10.1038/srep45292
85 Gupta, R., Badhe, Y., Mitragotri, S. and Rai, B. (2020) Permeation of nanoparticles across the intestinal lipid membrane: dependence on shape and surface chemistry studied through molecular simulations. *Nanoscale* **12**, 6318–6333 https://doi.org/10.1039/C9NR09947F
86 Živanović, V., Semini, G., Laue, M., Drescher, D., Aebischer, T. and Kneipp, J. (2018) Chemical mapping of leishmania infection in live cells by SERS microscopy. *Anal. Chem.* **90**, 8154–8161 https://doi.org/10.1021/acs.analchem.8b01451